Article

Study of Radiation Resistance to Helium Swelling of Li$_2$ZrO$_3$/LiO and Li$_2$ZrO$_3$ Ceramics

Baurzhan Abyshev [1], **Dmitriy I. Shlimas** [1,2,*], **Maxim V. Zdorovets** [1,2,3], **Yalkunzhan K. Arshamov** [4] **and Artem L. Kozlovskiy** [1,4]

1 Laboratory of Solid State Physics, The Institute of Nuclear Physics, Almaty 050032, Kazakhstan; baurzhan.abyshev@gmail.com (B.A.); mzdorovets@gmail.com (M.V.Z.); kozlovskiy.a@inp.kz (A.L.K.)
2 Engineering Profile Laboratory, L.N. Gumilyov Eurasian National University, Nur-Sultan 010008, Kazakhstan
3 Department of Intelligent Information Technologies, Ural Federal University, 620075 Yekaterinburg, Russia
4 Institute of Geology and Oil and Gas Business, Satbayev University, Almaty 050032, Kazakhstan; y.arshamov@satbayev.university
* Correspondence: shlimas@mail.ru; Tel./Fax: +7-7024-413368

Abstract: The key aim of this paper is to study the presence effect of LiO impurity phases in Li$_2$ZrO$_3$ ceramics on the resistance to helium swelling and structural degradation during implanted helium accumulation in the near-surface layer structure. The hypothesis put forward is based on a number of scientific papers, in which it was reported that the presence of two or more phases in lithium-containing ceramics led to a decrease in the rate of radiation damage and gas swelling due to the presence of additional interfacial boundaries that prevent the point defect accumulation. As a result of the evaluation of the crystal structure deformation, it was found that the presence of the LiO impurity phase in the structure of Li$_2$ZrO$_3$ ceramics led to a threefold decrease in the deformation of the crystal lattice due to helium swelling at doses of 5×10^{17}–5×10^{18} ion/cm^2. At the same time, the nature of the crystal lattice deformation for different ceramic types is different: in the case of Li$_2$ZrO$_3$ ceramics, an anisotropic distortion of the crystal structure is observed, in the case of Li$_2$ZrO$_3$/LiO ceramics, the crystal lattice deformation has an isotropic nature.

Keywords: helium swelling; radiation defects; lithium-containing ceramics; structure; helium ions

1. Introduction

To date, one of the promising areas of research in the field of search and creation of alternative energy sources is nuclear power, in particular, the development of new types of high-temperature reactors of a new generation that are capable of operating much longer than classical reactors. An important role in the development of nuclear energy is given to the search for new materials that, during their operation, will allow the production of additional fuel, such as tritium or hydrogen [1–3]. One of the ways to develop this area of research is the development related to the study of methods for obtaining lithium-containing ceramics, which have great prospects for the safe production of tritium and hydrogen, which is planned to be used in the future to create thermonuclear installations, as well as the transition to new types of nuclear fuel [4,5].

At the same time, as is known, the processes of tritium production in transmutation nuclear reactions of the ^{6}Li + n → He + T or D + T → He + n type lead to the fact that, in addition to tritium, transmutation helium can accumulate in the structure [6,7]. Due to its high mobility and low solubility, helium can agglomerate by forming He-V vacancies or fill voids in ceramics, thereby forming gas-filled bubbles leading to material destruction [8–10]. At the same time, the high mobility of vacancies leads to the formation of voids or pores in the structure, which can be filled with implanted helium at high concentrations.

The problem of helium accumulation in the structure of the near-surface layer and subsequent destruction processes has become quite acute in recent years among studies due

to the receipt of a large amount of new experimental data on the mechanisms of gaseous swelling of ceramics [11–15]. According to traditional models of gas swelling for metals, helium accumulation occurs near grain boundaries, followed by deformation of the crystal structure, and leads to the formation of blisters containing helium and exerting bursting pressure on the filled cavity. However, for ceramics with a complex crystal structure, anisotropic effects of structural damage and their further evolution play an important role in the gas swelling processes [16,17]. The presence of anisotropic effects associated with uneven radiation damage accumulation can have a significant effect on the processes of swelling and subsequent embrittlement of the damaged near-surface layer of ceramics. At the same time, the presence of two or more phases in the structure of ceramics can lead to the fact that the processes of radiation damage will be restrained by interfacial boundaries or a dislocation structure [18,19]. Such hypotheses were put forward in a number of works [20–23] devoted to the study of the properties of two-three-phase lithium-containing ceramics, according to which the presence of several phases in the structure affects not only the strengthening of ceramics but also their productivity in terms of helium yield, due to the acceleration of reactions with lithium [24,25].

It is also worth noting that despite the great interest in lithium-containing ceramics, as well as the study of their physic-chemical, structural, thermal conductive or mechanical properties, radiation damage plays an important role in their change, studies on which are currently insufficient to draw full conclusions and create a model describing their evolution.

The aim of this work is to study the radiation damage mechanisms depending on the implanted helium concentration, as well as to evaluate the effect of the presence of impurity phases in the structure of Li_2ZrO_3 ceramics on gaseous swelling and embrittlement of the near-surface layer.

2. Experimental Section

2.1. Sample Synthesis

All reagents used for the synthesis of the studied samples were purchased from Sigma Aldrich (Saint Louis, MI, USA). The chemical purity of the powders was 99.95%. Ceramics of the LiO/Li_2ZrO_3 and Li_2ZrO_3 types were obtained by solid-phase synthesis by mixing micron powders of $LiClO_4·3H_2O$ and ZrO_2 in a PULVERISETTE 6 classic planetary mill (Fritsch, Germany). The grinding of the samples was carried out in a grinding cup made of tungsten carbide at a grinding speed of 400 rpm for 1 h. During grinding, the temperature of the mixture was no more than 50–60 °C, which excludes any possibility of initialization of temperature phase transformations but does not exclude the possibility of phase transformations caused by mechanical action as a result of grinding. After stirring, the resulting mixtures were annealed at temperatures of 800 °C and 1000 °C. The choice of annealing temperatures was due to the results of [26], according to which, at given annealing temperatures, two-phase Li_2ZrO_3/LiO with a dominance of the Li_2ZrO_3 phase (800 °C) and single-phase close-packed Li_2ZrO_3 ceramics were formed.

2.2. Irradiation of Samples

Simulation of the radiation damage processes and the effect of helium swelling in lithium-containing ceramics was carried out using a low-energy He^{2+} (40 keV) ion flux obtained at the DC-60 heavy ion accelerator (Institute of Nuclear Physics, Nur-Sultan, Kazakhstan). Irradiation was carried out in a vacuum at a temperature of the target holder substrate of 25–30 °C. Irradiation fluence was 10^{15}–10^{18} ions/cm^2, ion flux density was 10^9 ions/cm^2·s, and ion current was no more than 40 nA. The choice of flux density was determined in order to prevent overheating of irradiated targets. The choice of irradiation fluences corresponds to the data, according to which, at doses above 10^{17} ion/cm^2, the formation of bubbles in the structure of the damaged layer is observed, which leads to the formation of blisters on the ceramic surface. According to the calculated data of SRIM Pro 2013, the energy losses of incident He^{2+} particles with an energy of 40 keV were $(dE/dx_{electron})$ 132.4 keV/µm during

collisions with electron shells, ($dE/dx_{nuclear}$) 5.5 keV/μm during collisions with nuclei, the maximum path length was 260–280 nm in the surface layer.

Figure 1 shows the simulation results of atomic displacements (dpa) along the trajectory of He^{2+} ions in the near-surface layer depending on irradiation fluence. The calculations were based on the SRIM Pro 2013 simulation data performed for the samples under study, taking into account the binding energy, as well as the density of the ceramics (4.58–4.31 g/cm^3).
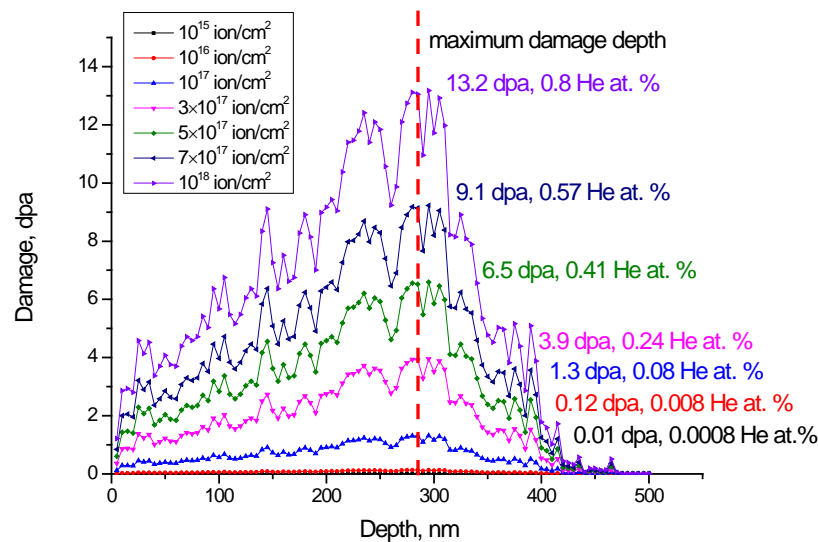

Figure 1. Simulation results of atomic displacements in the near-surface layer.

An analysis of the obtained data showed that at irradiation fluences of 10^{15}–10^{17} ion/cm^2, the displacements did not exceed 1.3 dpa, while at fluences above 5×10^{17} ion/cm^2, the displacements were more than 6.5 dpa. At the same time, the calculation of implanted helium concentration in the structure of the near-surface layer at the maximum radiation damage at high fluences was no more than 0.8–0.9 at. %.

2.3. X-ray Phase Analysis of the Studied Samples

The study of structural features, as well as the effects of radiation damage in the structure of ceramics, was carried out using the method of X-ray phase analysis. The implementation of these studies was carried out on a powder diffractometer D8 Advance ECO X-ray diffractometer (Bruker, Germany). The diffraction patterns were taken in the Bragg–Brentano mode, in the angular range of 2θ = 20–80°, with a step of 0.03°. The phase composition was determined by refining the contributions of diffraction reflections and the position of their maxima when compared with card values from the PDF-2 (2016) database. The crystal lattice parameters were refined using the DiffracEVA v.4.2 program code (Bruker, Germany).

The phase composition was determined by estimating the contributions of reflection areas for each phase and calculating their percentage using Formula (1):

$$V_{admixture} = \frac{RI_{phase}}{I_{admixture} + RI_{phase}} \tag{1}$$

where I_{phase}—average integrated intensity of the main phase of the diffraction line, $I_{admixture}$—the average integrated intensity of the additional phase, R = 1.45.

2.4. Determination of Thermal Conductive Properties

The thermal conductive properties were determined using a KIT-800 (Moscow, Russia) thermal conductivity measuring device, which was based on the method of changing the

temperature difference of the sample with a longitudinal heat flow through the sample in the case of heating. The thermal conductivity coefficient (λ, W/(m·K)) was determined using Expression (2) based on the change in temperature and heat flux density:

$$\lambda = \frac{q\delta}{t_{c1} - t_{c2}} \qquad (2)$$

where q is the heat flux density, W/m^2; t_{c1} and t_{c2} are the temperatures on both sides of the sample, K; δ is the thickness of the sample, m.

3. Results and Discussion

3.1. Characterization of Initial Samples

Figure 2 shows the results of X-ray phase analysis of the studied samples before irradiation, which were obtained at different annealing temperatures. As can be seen from the presented data, in the case of the sample obtained at an annealing temperature of 800 °C, the diffraction pattern contains low-intensity peaks characteristic of the LiO hexagonal phase (PDF-00-009-0355), with characteristic crystal lattice parameters: a = 3.1186 Å, c = 7.6109 Å, V = 64.11 Å^3. At the same time, the dominant phase in the structure of ceramics is the monoclinic phase Li$_2$ZrO$_3$ (PDF-01-070-8744), with the crystal lattice parameters: a = 5.3921 Å, b = 8.9029 Å, c = 5.3625 Å, β = 111.907°, V = 238.80 Å^3. After evaluating the contributions of each intense phase, it was found that the ratio of the Li$_2$ZrO$_3$/LiO phases was approximately 90/10. According to the crystallographic density calculations using Formula (3), it was found that the density of the Li$_2$ZrO$_3$/LiO ceramics was 4.258 g/cm^3.

$$p = \frac{1.6602\sum AZ}{V_o} \qquad (3)$$

where Z is the number of atoms in a crystal cell, A is the atomic weight of atoms.

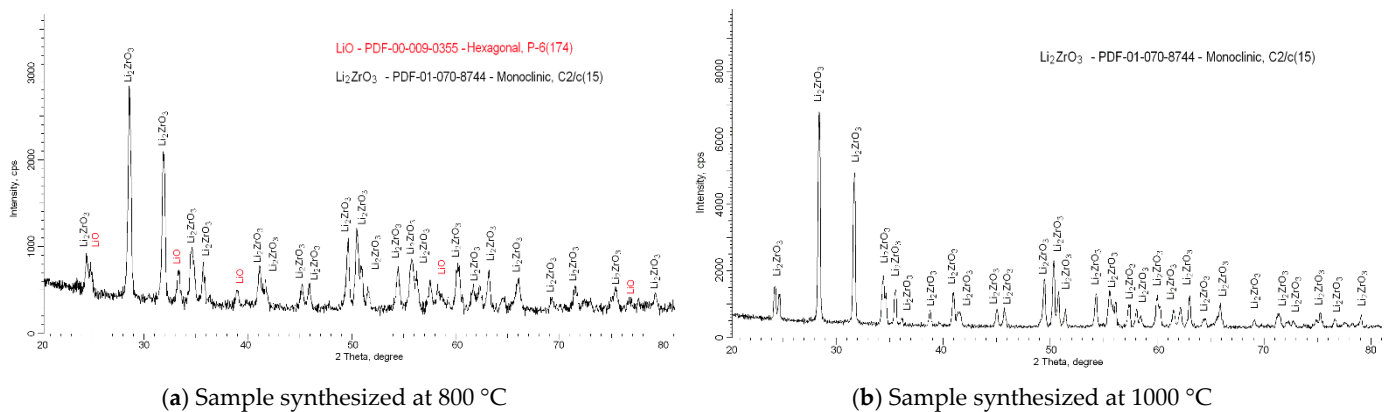(**a**) Sample synthesized at 800 °C (**b**) Sample synthesized at 1000 °C

Figure 2. Results of X-ray phase analysis of the studied samples.

For the sample obtained at an annealing temperature of 1000 °C, the presence of peaks characteristic of the LiO phase was not found, which indicates a complete phase transformation of the Li$_2$ZrO$_3$ phase under the selected synthesis conditions. The crystal lattice parameters for the sample were a = 5.3625 Å, b = 8.8611 Å, c = 5.3415 Å, β = 111.601°, V = 235.91 Å^3, the density was 4.309 g/cm^3. At the same time, comparing the crystal lattice parameters for samples obtained at different annealing temperatures, we can conclude that the displacement of the LiO phase leads to structural ordering and densification of ceramics. The ceramic density increase leads to a decrease in crystalline porosity, which was 1.2% for Li$_2$ZrO$_3$/LiO, while for Li$_2$ZrO$_3$ ceramics, the porosity was 0.9%. The calculation of porosity was carried out based on the results of crystal density changes.

Analyzing the shape of diffraction lines using the Williamson–Hall method, which makes it possible to evaluate the influence of the size and deformation effects arising in

the structure of ceramics as a result of synthesis, the following was established. For the samples obtained at a temperature of 800 °C, the influence of the deformation contribution in the structure was somewhat larger than the size contribution (the lines of the diffraction patterns have an asymmetric shape). At the same time, the size of crystallites for these ceramics was about 28–30 nm. For samples obtained at a temperature of 1000 °C, the size and deformation contributions were equally probable, while the shape of the diffraction peaks was more symmetrical, and the crystallite size was about 40–45 nm. An increase in the size of crystallites indicates an enlargement of ceramics, accompanied by a change in the dislocation density in the structure.

3.2. Determination of Gas Swelling of the Crystal Lattice

As is known, irradiation with low-energy ions, in particular, helium or hydrogen, leads to radiation damage accumulation in the near-surface layer, associated with the formation of vacancy defects, such as He-V, which are capable of agglomerating and filling pores. Such agglomeration can lead to additional deformations and distortions of the crystal structure, and at high concentrations of implanted helium, gas-filled bubbles or blisters can form both on the ceramic surface and inside the damaged layer. The degree of radiation resistance to swelling can be assessed by analyzing X-ray diffraction data, which, based on data on changes in the shape of diffraction lines, their position and intensity make it possible to estimate with high accuracy the structural changes caused by irradiation. At the same time, the distortions of structural parameters depending on the irradiation fluence, as well as the determination of various contributions to the change in X-ray diffraction patterns, make it possible to evaluate the evolution of the crystal structure and the mechanisms that affect its changes.

Analysis of the X-ray data of the studied samples did not reveal the formation of new diffraction reflections, which indicates the absence of phase transformation processes as a result of irradiation. The main changes occur only due to the displacement of reflections, as well as a change in their intensity and shape, which indicates deformation and distorting processes caused by irradiation.

Table 1 presents the results of changing the crystal lattice parameters for the samples under study depending on the irradiation fluence for the samples under study.

Table 1. Data of structural parameters of the crystal lattice.

Irradiation Fluence, ion/cm^2	Ceramic Type		
	Li_2ZrO_3/LiO		Li_2ZrO_3
	Crystal Lattice Parameters, Å		
Phase Concentration:	90/10		100
Phase	Li_2ZrO_3—Monoclinic C2/c(15)	LiO—Hexagonal P-6(174)	Li_2ZrO_3—Monoclinic C2/c(15)
Pristine sample	a = 3.1186, c = 7.6109, V = 64.11 Å^3	a = 5.3921, b = 8.9029, c = 5.3625, β = 111.907°, V = 238.81 Å^3	a = 5.3625, b = 8.8611, c = 5.3415, β = 111.607°, V = 235.91 Å^3
10^{15}	a = 3.1199, c = 7.6170, V = 64.21 Å^3	a = 5.3942, b = 8.9056, c = 5.3715, β = 111.954°, V = 239.33 Å^3	a = 5.3673, b = 8.8716, c = 5.3474, β = 111.609°, V = 236.61 Å^3
10^{16}	a = 3.1236, c = 7.6231, V = 64.41 Å^3	a = 5.3975, b = 8.9127, c = 5.3758, β = 111.997°, V = 239.79 Å^3	a = 5.3737, b = 8.8858, c = 5.3559, β = 111.780°, V = 237.49 Å^3
10^{17}	a = 3.1273, c = 7.63524, V = 64.67 Å^3	a = 5.4018, b = 8.9162, c = 5.3728, β = 112.041°, V = 239.86 Å^3	a = 5.3801, b = 8.9035, c = 5.3645, β = 111.891°, V = 238.44 Å^3
3×10^{17}	a = 3.1311, c = 7.6474, V = 64.93 Å^3	a = 5.4061, b = 8.9269, c = 5.3771, β = 112.131°, V = 240.38 Å^3	a = 5.3887, b = 8.9178, c = 5.3731, β = 111.980°, V = 239.43 Å^3
5×10^{17}	a = 3.1373, c = 7.6627, V = 65.32 Å^3	a = 5.4105, b = 8.9341, c = 5.3793, β = 112.221°, V = 240.71 Å^3	a = 5.3973, b = 8.9391, c = 5.3816, β = 112.070°, V = 240.62 Å^3
7×10^{17}	a = 3.1436, c = 7.6841, V = 65.76 Å^3	a = 5.4169, b = 8.9448, c = 5.3901, β = 112.401°, V = 241.56 Å^3	a = 5.4102, b = 8.9677, c = 5.3966, β = 112.249°, V = 242.34 Å^3
10^{18}	a = 3.1473, c = 7.6964, V = 66.02 Å^3	a = 5.4234, b = 8.9662, c = 5.4007, β = 112.535°, V = 242.57 Å^3	a = 5.4211, b = 8.9963, c = 5.4117, β = 112.429°, V = 243.96 Å^3

A general analysis of changes in the structural parameters of the crystal lattice, as well as its volume, indicates the nature of the deformation of the crystal lattice, which in this

case of irradiation is caused by tensile stresses and tensile deformation. This is evidenced by a dose increase in the parameters, as well as in the crystal lattice volume.

Figure 3 shows the comparative results of the crystal lattice deformation for the Li$_2$ZrO$_3$ monoclinic phase depending on the irradiation fluence for both types of ceramics under study. The analysis was carried out by calculating the deformation of the crystal lattice parameters along all axes in comparison with the parameters of the initial samples used for further irradiation. The results are presented on a single scale for ease of comparison of relative changes in the crystal lattice deformation.
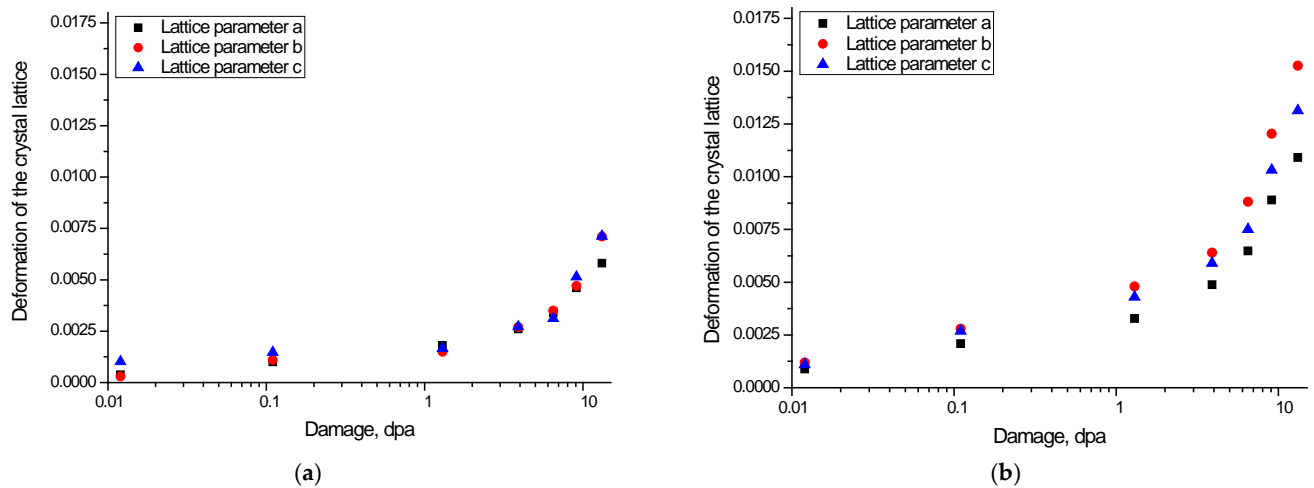

(a)

(b)

Figure 3. Results of deformation distortions of the crystal lattice parameters for the Li$_2$ZrO$_3$ monoclinic phase depending on the irradiation dose (displacement values are presented on a logarithmic scale): (**a**) Li$_2$ZrO$_3$/LiO ceramics; (**b**) Li$_2$ZrO$_3$ ceramics.

The deformation of the crystal lattice (DCL) was estimated using the following Equations (4)–(6), which reflect the change in the value of the parameters of the crystal lattice along the axis, and also characterize its distortion as a result of external influences.

$$DCL(a) = \frac{a_{irr} - a_0}{a_0} \tag{4}$$

$$DCL(b) = \frac{b_{irr} - b_0}{b_0} \tag{5}$$

$$DCL(c) = \frac{c_{irr} - c_0}{c_0} \tag{6}$$

a_{irr}, b_{irr}, c_{irr}—crystal lattice parameters of irradiated samples, a_0, b_0, c_0—crystal lattice parameters of the initial samples.

For samples of Li$_2$ZrO$_3$/LiO ceramics, the deformation distortion of the crystal lattice parameters depending on the irradiation fluence has a character of tensile deformation close to an isotropic change along all axes. At the same time, at irradiation fluences of 10^{15}–10^{17} ions/cm^2, deformation changes have a small increase, which indicates resistance to deformation resulting from the accumulation of radiation damage. With an increase in the irradiation fluence above 3×10^{17} ion/cm^2, for which, as is known from the literature [27,28], the processes of helium bubble formation due to an increase in implanted helium concentration are characteristic, an increase in lattice deformation is observed.

In the case of Li$_2$ZrO$_3$ ceramic samples, an increase in the irradiation fluence leads to an anisotropic lattice distortion, which is expressed as a difference in the relative values of the crystal lattice deformation. The anisotropic nature of the deformation of the crystal lattice indicates that the accumulation of radiation damage leads to destabilization of the crystal lattice, as well as its partial disordering. At the same time, this disorder is more

pronounced along the b and c axes. This behavior of deformation can be due to different binding energies of atoms, as well as their positions in the lattice sites.

Comparing the results of crystal lattice deformation at maximum irradiation fluences, it was found that the presence of the LiO impurity phase in the structure of Li_2ZrO_3 ceramics leads to a threefold decrease in the crystal lattice deformation. At the same time, the nature of the crystal lattice deformation for different types of ceramics is different: in the case of Li_2ZrO_3 ceramics, an anisotropic crystal structure distortion is observed, in the case of Li_2ZrO_3/LiO ceramics, the deformation of the crystal lattice has an isotropic character.

Figure 4 shows the results of changes in the porosity of ceramics depending on irradiation dose, which indicates a deterioration in the density and disorder of the structure.
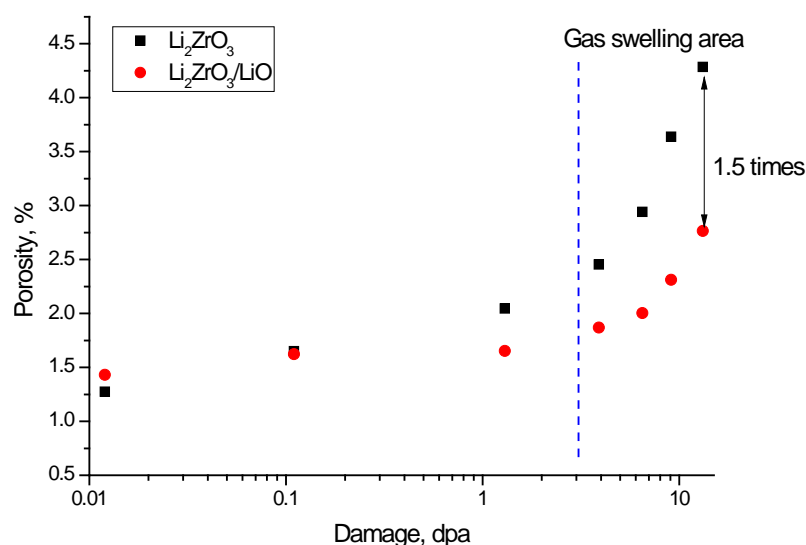

Figure 4. Results of changes in the porosity of ceramics depending on irradiation dose.

As can be seen from the data presented, at small displacement values typical for irradiation fluences of 10^{15}–10^{17} ion/cm^2, the porosity of Li_2ZrO_3/LiO ceramics practically does not change, which is due to the high resistance to structural deformations because of the presence of impurity phases. At the same time, for Li_2ZrO_3 ceramics, the increase in porosity at large displacements occurs according to an exponential law with a sharp increase in porosity, which indicates the formation of voids in the ceramic structure due to deformation and distorting processes of the crystal lattice.

Figure 5 shows the results of the change in the crystal lattice volume depending on the irradiation dose, which characterizes the effect of ceramic swelling as a result of the radiation damage accumulation during helium implantation.

The general form of changes indicates that the accumulation of radiation damage in the structure of ceramics leads not only to tensile deformation of the crystal lattice but also to its swelling. In this case, the swelling rate trend depending on the irradiation fluence is different for both types. In the case of Li_2ZrO_3/LiO ceramics, the most pronounced swelling effects are observed at irradiation fluences above 5×10^{17} ion/cm^2, for which the swelling of the crystal lattice is more than 1%. At fluences of 10^{15}–10^{17} ion/cm^2, the swelling value is no more than 0.5%. For Li_2ZrO_3 ceramics, the trend of change in the swelling rate is close to linear depending on the irradiation dose, while at high irradiation fluences of 7×10^{17}–7×10^{18} ion/cm^2, the lattice swelling exceeds 3%, which is 2.5 times greater than the similar value for Li_2ZrO_3/LiO ceramics.

Thus, we can conclude that the presence of the LiO phase in the structure of ceramics leads not only to a decrease in the deformation of the crystal lattice but also to a decrease in the effect of swelling of the crystal lattice. This may be due to several factors.

First, the presence of the LiO impurity phase creates additional interphase boundaries that prevent helium migration and the formation of complex defects of the He-V type.
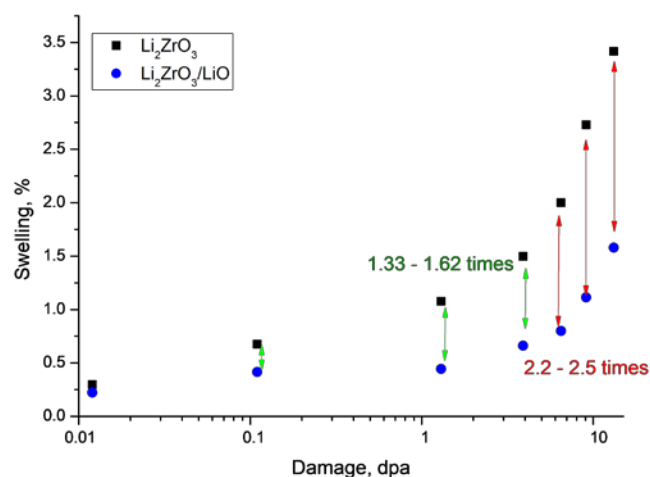
Figure 5. Results of the crystal lattice swelling depending on the irradiation dose (displacement values are presented on a logarithmic scale).

Second, an analysis of the crystallite sizes in the initial state indicated that the dislocation density for Li_2ZrO_3/LiO ceramics is much higher than for Li_2ZrO_3 ceramics, which is related to the difference in crystallite sizes. The presence of a high density of dislocations, as shown in [27,28], leads to the creation of additional obstacles to helium agglomeration in voids with the subsequent formation of gas-filled bubbles, thereby reducing the swelling of the crystal lattice.

Thirdly, the anisotropic deformation of the crystal lattice for Li_2ZrO_3 ceramics leads to a sharp deterioration in the structural properties of ceramics at high irradiation fluences, as well as a large number of broken crystal and chemical bonds in the structure, resulting in free vacancy defects and primary knocked-on atoms that can also interact with helium.

3.3. Results of Changes in Thermal Conductivity

An important factor in assessing the applicability of ceramics as structural materials for nuclear reactors, as well as their use for breeding tritium, is the long-term preservation of the thermal conductivity of ceramics, which depends on many factors, including radiation damage and swelling. As is known, the swelling processes are directly related to the processes of changes in density and porosity, which in turn leads to a deterioration in heat removal from the structure and the occurrence of overheating, which can have negative consequences on the material properties. Figure 6 shows the results of changes in the thermal conductivity coefficient for the studied ceramics depending on the irradiation fluence.

Differences in coefficients in the initial state are due to the presence of structural distortions in Li_2ZrO_3/LiO ceramics due to the presence of the LiO impurity phase, as well as to the deformation of the crystal lattice. The change in the thermal conductivity coefficient depending on the irradiation fluence can be divided into two main stages, which are characterized by different trends and are associated with structural distortions. The first stage is characterized by small changes in the thermal conductivity coefficients and their decrease with increasing irradiation fluence. At the same time, for Li_2ZrO_3/LiO ceramics, the change in the coefficients depending on the irradiation fluence is practically not observed for irradiation fluences of 10^{15}-10^{17} ion/cm^2. The value of the difference in thermal conductivity coefficients for two types of ceramics at given irradiation fluences is no more than $\Delta = 0.008$.

For irradiation fluences above 5×10^{17} ion/cm^2, there is a sharp change in the trend of thermal conductivity coefficient decrease, which is due to the formation of deformation distortions in the structure, as well as crystal lattice swelling, which leads to a change in porosity and the formation of bubbles in the damaged layer structure. At the same time, for Li_2ZrO_3 ceramics, the deterioration of thermal conductive properties is more pronounced

than for Li_2ZrO_3/LiO ceramics, which is due to smaller structural changes caused by irradiation, as well as smaller values of crystal lattice swelling as a result of irradiation.
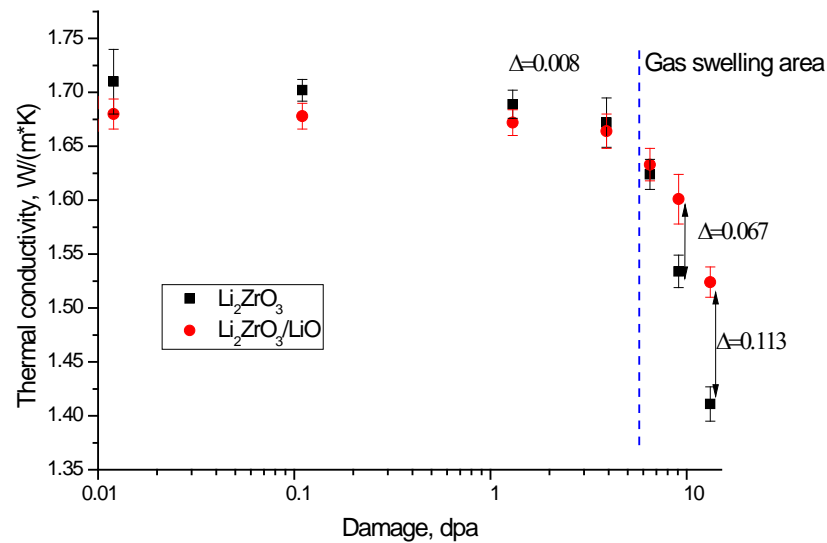

Figure 6. Results of changes in the thermal conductivity coefficient of ceramics depending on the irradiation dose (displacement values are presented on a logarithmic scale).

3.4. Results of Changes in Strength Properties

Figure 7 shows the results of changes in microhardness of damaged near-surface layer of ceramics depending on irradiation fluence.
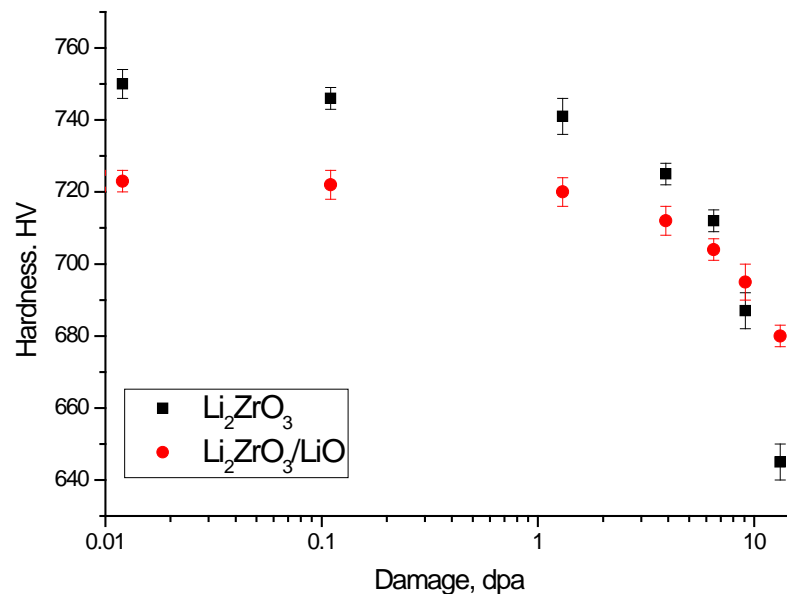

Figure 7. Results of changes in the microhardness of ceramics depending on the value of atomic displacements (displacement values are presented on a logarithmic scale).

It can be seen from the data presented that in the case of Li_2ZrO_3 ceramics, the initial hardness is 4% higher than for Li_2ZrO_3/LiO ceramics, which is due to higher density and lower porosity. However, for irradiated samples, the change in the microhardness of the damaged layer has a different trend. Thus, for samples of Li_2ZrO_3 ceramics, a sharp decrease in microhardness is observed at irradiation fluences above 10^{17} ion/cm^2 (more than 4 dpa) and is more than 5%, and at the maximum irradiation dose (13.2 dpa), the softening of the damaged layer is more than 14%, which indicates strong destruction of

the near-surface layer caused by irradiation and accumulation of radiation damage. In the case of Li_2ZrO_3/LiO ceramics, the presence of an impurity phase leads to an increase in the resistance to degradation of strength properties, as well as a decrease in the softening degree of the damaged layer by more than 2.5 times at the maximum irradiation dose.

4. Conclusions

The paper presents the results of changes in the structural properties and thermal conductivity of Li_2ZrO_3 ceramics subjected to irradiation with He^{2+} ions with fluences of 10^{15}–10^{18} ion/cm^2, which correspond to atomic displacements from 0.01 to 13.2 dpa. The methods of X-ray phase analysis, as well as the method of determining the longitudinal heat flux, were used as the main research methods. During the studies, it was found that the presence of the LiO impurity phase in the structure of Li_2ZrO_3 ceramics leads to a decrease in the deformation distortions of the crystal lattice, as well as a decrease in the degree of swelling of the crystal structure as a result of the accumulation of implanted helium in the ceramic structure. It has been established that for Li_2ZrO_3 ceramics without an impurity phase, crystal structure distortions are anisotropic in nature, which leads to crystal lattice swelling at irradiation fluences of 5×10^{17}–5×10^{18} ion/cm^2 by 3.0–3.5% of the initial volume. During the measurement of the thermal conductive characteristics, it has been found that lithium-containing ceramics have high resistance to decrease the thermal conductive properties at irradiation fluences of 10^{15}–10^{17} ion/cm^2. At the same time, accumulation of radiation damages in structure leads to deterioration of thermal conductivity due to change of structural characteristics, a decrease of ceramic density associated with an increase of crystal lattice volume, and an increase of porosity.

Author Contributions: Conceptualization, M.V.Z., B.A. and A.L.K.; methodology, B.A., D.I.S. and A.L.K.; formal analysis, Y.K.A., D.I.S. and M.V.Z.; investigation, B.A., A.L.K. and M.V.Z.; resources, M.V.Z.; writing—original draft preparation, review, and editing, B.A., M.V.Z. and A.L.K.; visualization, M.V.Z.; supervision, M.V.Z. All authors have read and agreed to the published version of the manuscript.

Institutional Review Board Statement: Not applicable.

Informed Consent Statement: Not applicable.

Data Availability Statement: Not applicable.

Conflicts of Interest: The authors declare that they have no conflict of interest.

References

1. Ekberg, C.; Costa, D.R.; Hedberg, M.; Jolkkonen, M. Nitride fuel for Gen IV nuclear power systems. *J. Radioanal. Nucl. Chem. Artic.* **2018**, *318*, 1713–1725. [CrossRef] [PubMed]
2. Yanez, J.; Class, A.G. Analysis of the accuracy of residual heat removal in gen-IV reactors. *Nucl. Eng. Des.* **2021**, *376*, 111102. [CrossRef]
3. Thomas, J.-B.; Anzieu, P.; Lenain, R. The place and the potential of LightWater Reactors in the transition from Gen-III to Gen-IV. In *Nuclear Reactor Systems*; EDP Sciences: Les Ulis, France, 2021; pp. 261–322.
4. Bertrand, F.; Marie, N.; Bachrata, A.; Droin, J.-B.; Manchon, X. Simplified thermohydraulic criteria for a comparison of the accidental behaviour of GEN IV nuclear reactors and of PWRs. In Proceedings of the 18th International Topical Meeting on Nuclear Reactor Thermal Hydraulics (NURETH-18), Portland, OR, USA, 18–22 August 2019; pp. 2483–2496.
5. Kotomin, E.; Kuzovkov, V.; Popov, A.; Vila, R. Kinetics of F center annealing and colloid formation in Al2O3. *Nucl. Instruments Methods Phys. Res. Sect. B Beam Interactions Mater. Atoms* **2016**, *374*, 107–110. [CrossRef]
6. Koga, Y.; Matsuura, H.; Katayama, K.; Otsuka, T.; Goto, M.; Hamamoto, S.; Ishitsuka, E.; Nakagawa, S.; Tobita, K.; Konishi, S.; et al. Effect of nuclear heat caused by the 6Li(n,α)T reaction on tritium containment performance of tritium production module in High-Temperature Gas-Cooled reactor for fusion reactors. *Nucl. Eng. Des.* **2021**, *386*, 111584. [CrossRef]
7. Averback, R.S.; Ehrhart, P.; Popov, A.I.; Sambeek, A.V. Defects in ion implanted and electron irradiated Mgo and Al_2O_3. *Radiat. Eff. Defects Solids* **1995**, *136*, 169–173. [CrossRef]

8. Lisitsyn, V.M.; Lisitsyna, L.A.; Popov, A.I.; Kotomin, E.A.; Abuova, F.U.; Akilbekov, A.; Maier, J. Stabilization of primary mobile radiation defects in MgF_2 crystals. *Nucl. Instrum. Methods Phys. Res. Sect. B Beam Interact. Mater. At.* **2016**, *374*, 24–28. [CrossRef]

9. Kadyrzhanov, K.K.; Tinishbaeva, K.; Uglov, V.V. Investigation of the effect of exposure to heavy Xe22+ ions on the mechanical properties of carbide ceramics. *Eurasian Phys. Tech. J.* **2021**, *17*, 46–53. [CrossRef]

10. Lushchik, A.; Lushchik, C.; Vasil'Chenko, E.; Popov, A.I. Radiation creation of cation defects in alkali halide crystals: Review and today's concept (Review Article). *Low Temp. Phys.* **2018**, *44*, 269–277. [CrossRef]

11. Tynyshbayeva, K.M.; Kadyrzhanov, K.K.; Kozlovskiy, A.L.; Kuldeyev, Y.I.; Uglov, V.; Zdorovets, M.V. Study of Helium Swelling and Embrittlement Mechanisms in SiC Ceramics. *Crystals* **2022**, *12*, 239. [CrossRef]

12. Shlimas, D.I.; Kozlovskiy, A.L.; Syzdykov, A.K.; Borgekov, D.B.; Zdorovets, M.V. Study of Resistance to Helium Swelling of Lithium-Containing Ceramics under High-Temperature Irradiation. *Crystals* **2021**, *11*, 1350. [CrossRef]

13. Kotomin, E.; Kuzovkov, V.; Popov, A.I. The kinetics of defect aggregation and metal colloid formation in ionic solids under irradiation. *Radiat. Eff. Defects Solids* **2001**, *155*, 113–125. [CrossRef]

14. Gu, S.; Ji, B.; Qi, Q.; Wang, J.; Zhou, H.-S.; Zhang, Y.; Luo, G.-N. Effects of He irradiation on the microstructure and mechanical performance of Li2TiO3. *Nucl. Fusion* **2021**, *61*, 106035. [CrossRef]

15. Wang, C.; Tu, H.; Su, R.; Gao, J.; King, B.V.; O'Connor, D.J.; Shi, L. Annealing effects on the structure and hardness of helium-irradiated Cr_2AlC thin films. *J. Am. Ceram. Soc.* **2021**, *104*, 593–603. [CrossRef]

16. Abyshev, B.; Kozlovskiy, A.L.; Zhumadilov, K.S.; Trukhanov, A.V. Study of Radiation Embitterment and Degradation Processes of Li_2ZrO_3 Ceramic under Irradiation with Swift Heavy Ions. *Ceramics* **2022**, *5*, 2. [CrossRef]

17. Wang, J.; Xu, Y.; Liu, H.-D.; Xiang, M.; Zhou, H.; Zhang, Y.; Luo, G.-N.; Qi, Q. Influence of ion irradiations on the microstructure in the tritium breeder material Li_2TiO_3. *Nucl. Instruments Methods Phys. Res. Sect. B Beam Interactions Mater. Atoms* **2019**, *450*, 189–194. [CrossRef]

18. Yang, S.; Nakagawa, Y.; Kondo, M.; Shibayama, T. Anisotropic defect distribution in He+-irradiated 4H-SiC: Effect of stress on defect distribution. *Acta Mater.* **2021**, *211*, 116845. [CrossRef]

19. Yang, S.; Nakagawa, Y.; Kondo, M.; Shibayama, T. Electron energy-loss spectroscopic evaluation of depth-dependent swelling of He+ ion-irradiated 4H-SiC correlated with defect type. *J. Appl. Phys.* **2020**, *127*, 175106. [CrossRef]

20. Cipa, J.; Zarins, A.; Supe, A.; Kizane, G.; Zolotarjovs, A.; Baumane, L.; Trinkler, L.; Leys, O.; Knitter, R. X-ray induced defects in advanced lithium orthosilicate pebbles with additions of lithium metatitanate. *Fusion Eng. Des.* **2019**, *143*, 10–15. [CrossRef]

21. Qi, Q.; Wang, J.; Zhou, Q.; Zhang, Y.; Zhao, M.; Gu, S.; Nakata, M.; Zhou, H.; Oya, Y.; Luo, G.-N. Comparison of tritium release behavior in Li_2TiO_3 and promising core-shell Li_2TiO_3–Li_4SiO_4 biphasic ceramic pebbles. *J. Nucl. Mater.* **2020**, *539*, 152330. [CrossRef]

22. Rao, G.J.; Mazumder, R.; Bhattacharyya, S.; Chaudhuri, P. Fabrication of Li_4SiO_4-Li_2ZrO_3 composite pebbles using extrusion and spherodization technique with improved crush load and moisture stability. *J. Nucl. Mater.* **2019**, *514*, 321–333.

23. Yang, M.; Gong, Y.; Ran, G.; Wang, H.; Chen, R.; Huang, Z.; Shi, Q.; Chen, X.; Lu, T.; Xiao, C. Tritium release behavior of Li_4SiO_4 and Li_4SiO_4 + 5 mol% TiO2 ceramic pebbles with small grain size. *J. Nucl. Mater.* **2019**, *514*, 284–289. [CrossRef]

24. Yang, M.; Zhao, L.; Ran, G.; Gong, Y.; Wang, H.; Peng, S.; Xiao, C.; Chen, X.; Lu, T. Tritium release behavior of Li_2TiO_3 and $2Li_2TiO_3$-Li_4SiO_4 biphasic ceramic pebbles fabricated by microwave sintering. *Fusion Eng. Des.* **2021**, *168*, 112390. [CrossRef]

25. Qi, Q.; Ji, B.; Gu, S.; Zhang, Y.; Zhou, H.; Luo, G.-N. Annihilation behavior of irradiation defects induced by γ-ray in biphasic tritium breeding materials xLi_2TiO_3-(1-x) Li_4SiO_4. *Ceram. Int.* **2021**, *47*, 434–438. [CrossRef]

26. Zdorovets, M.V.; Kozlovskiy, A.L.; Abyshev, B.; Yensepbayev, T.A.; Uzbekgaliyev, R.U.; Shlimas, D.I. Study of Phase Formation Processes in Li2ZrOCeramics Obtained by Mechanochemical Synthesis. *Crystals* **2022**, *12*, 21. [CrossRef]

27. Zhang, H.; Su, R.; Szlufarska, I.; Shi, L.; Wen, H. Helium effects and bubbles formation in irradiated Ti_3SiC_2. *J. Eur. Ceram. Soc.* **2020**, *41*, 252–258. [CrossRef]

28. Liu, Y.; Zhu, Y.; Shen, T.; Chai, J.; Niu, L.; Li, S.; Jin, P.; Zheng, H.; Wang, Z. Irradiation response of Al_2O_3-ZrO_2 ceramic composite under He ion irradiation. *J. Eur. Ceram. Soc.* **2021**, *41*, 2883–2891. [CrossRef]